HETEROCYCLES, Vol. 98, No. 12, 2019, pp. 1707 - 1724. © 2019 The Japan Institute of Heterocyclic Chemistry
Received, 6th November, 2019, Accepted, 25th December, 2019, Published online, 7th January, 2020
DOI: 10.3987/COM-19-14184

SYNTHESIS, CHARACTERIZATION, AND ELECTRONIC AND STRUCTURAL CALCULATIONS OF SOME 1,4-DISUBSTITUTED CYCLOPENTA[*d*][1,2]OXAZINES

Nathan C. Tice,[1]* Steven Wild,[1] Christian Olmstead,[1] Edwin D. Stevens,[2] Bangbo Yan,[2] Hannah Brooks,[2] and Judith L. Jenkins[3]

1. Department of Physical Sciences, University of Findlay, 1000 N. Main Street, Findlay, Ohio, 45840, USA, tice@findlay.edu
2. Department of Chemistry, Western Kentucky University, 1906 College Heights Blvd. Bowling Green, KY 42101, USA
3. Department of Chemistry, Eastern Kentucky University, 521 Lancaster Avenue, Richmond, KY 40475, USA

Abstract – Our current work focuses upon the formation and characterization of some 1,4-disubstituted cyclopenta[*d*][1,2]oxazines via ring closure with hydroxyl-amine on a 1,2-diacyl cyclopentadiene precursor. Recently, we formed and characterized two fused-ring disubstituted oxazines (R = thienyl, 4-chlorophenyl) in high yield, which serve as precursors towards oxazine-based conducting polymers. X-Ray crystallographic analysis of the thienyl oxazine did show favorable π-π stacking, critical to effective intermolecular charge transfer. To further evaluate its electronic and optical properties, theoretical calculations were performed on the thienyl oxazine, including Natural Bond Orbital analysis. Calculated values suggest a strong potential for Non-Linear Optical applications.

INTRODUCTION

Heterocycles and their related fused-ring analogs comprise an important class of organic compounds and offer a wide range of applications that include biological, industrial, and materials applications.[1-6] When these heterocycles are incorporated into conducting polymers, many display semiconducting properties when doped. Of the catalog of organic heterocycles available, polythiophene and polypyrrole (Figure 1 A, B) and their derivatives are the most heavily utilized. These so called “plastic electronics” offer a pathway towards novel and straightforward device fabrication.[7] Furthermore, polythiophenes tend to

display higher environmental stability and structural versatility compared to other heterocyclic-based materials.[8,9] Recent advances in molecular and polymer based electronic devices have included organic light-emitting diodes (OLEDS), field-effect transistors (FETs),[10] and organic photovoltaic (OPV) cells.[11]

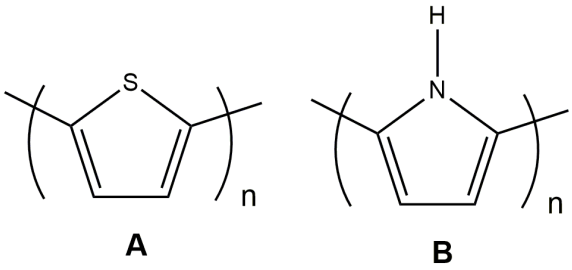

Figure 1. Polythiophene (**A**) and polypyrrole (**B**)

While thiophenes have been more thoroughly scrutinized and utilized as novel electronic materials, oxazines are a similar class of heterocycles of interest because of their ubiquity in nature and unique optical and electronic properties. Oxazines are 6-membered rings containing a nitrogen and oxygen atom within the heterocyclic ring (Figure 2). Oxazines that contain aromatic fragments like fused a cyclopentadienyl ring (cyclopenta[*d*][1,2] fused-ring oxazines, Figure 2 **B**) are well known and possess a wide variety of novel biological and pharmaceutical applications.[12-19] While similar heterocyclic systems that contain a mixture of heteroatoms (e.g., N and S) have been utilized as voltage-sensitive dyes,[20] there is a strong potential for oxazines specifically to be utilized in materials applications. Recently, cobalt(II) spirooxazine-based materials have been shown to display photomagnetic properties useful for quantum data storage and processing.[21] Oxazine-based dyes have also been employed as effective electron acceptors when paired with novel electron storage materials, such as single wall carbon nanotubes (SWCNTs), for applications in photovoltaic cells and fuel cells.[22] Additionally, a large class of spiroindolinonaphthoxazines have been reported and shown to display significant photochromic properties.[23] Furthermore, benzoxazines can form a variety of thermoset polymers with favorable properties, including thermal and flame stability and high mechanical performance.[24]

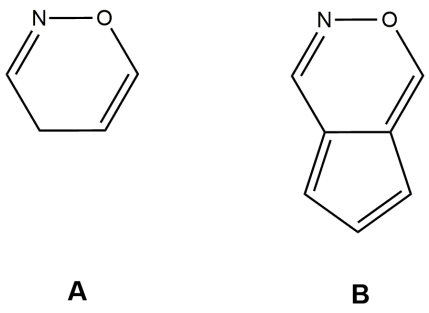

Figure 2. 4*H*-1,2-Oxazine (**A**) and cyclopenta[*d*][1,2]oxazine (**B**)

Our primary interest is in oxazine derivatives and other alternative heterocycles as foundational structures for electronic materials that possess novel electronic or optical properties (e.g., Non-Linear Optical or NLO materials). We have previously reported upon the formation of a series 5,6-fused oxazines that incorporate a Cp moiety (Scheme 1). This route, initially reported by Linn and Sharkey, is accomplished by ring closure of a simple 1,2-diacylcyclopentadiene precursor with hydroxylamine.[25] Linn and Sharkey only reported oxazines where aryl rings (e.g., phenyl and tolyl) were employed as the substituents at the 1- and 4-postions and with negligible spectroscopic evidence. However, we expanded this series to other substituent types to see how general the reaction conditions were and formed a variety of heterocyclic substituted cased, including thienyl and furyl cases.[26] Formation of additional alkyl and aryl substituted oxazines was accomplished with reasonable yields (28.5-45.8%) under those conditions first reported by Linn and Sharkey. We also examined thoroughly the solid-state nature of

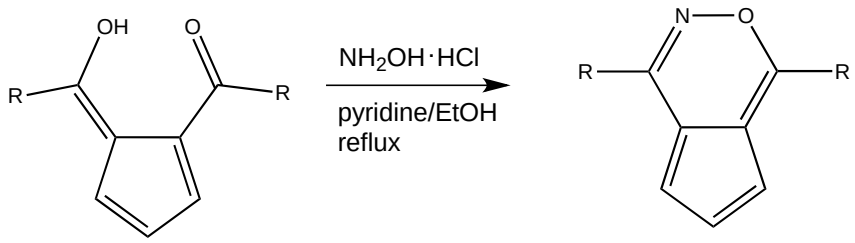

Scheme 1. Formation of 1,4-disubstituted cyclopentaoxazines

these 5,6-fused oxazines and did find that favorable π-stacking was observed suggesting that these materials would be adaptable towards device incorporation. Our recent work has focused upon the formation and investigation of 5,6-fused oxazines that could be incorporated into conducting polymers, namely via transition metal coupling reactions or electrochemical polymerization. These two techniques are widely utilized in the formation of conducting heterocyclic polymers.[27] Our long term goal would be to incorporate novel oxazine moieties into a more traditional thiophene polymer frameworks and form a unique mixed heterocyclic conducting material (Figure 3). Furthermore, we wished to perform computational studies on oxazine monomers that could actually be incorporated into a future conducting polymer. This sort of modeling would more effectively help us understand the electronic and optical nature of cyclopentaoxazines and their potential role in digital devices. Herein, we report upon the formation and characterization of two 1,4-disubstituted cyclopenta[*d*][1,2]oxazines conducting polymer precursors containing the thienyl and 4-chlorophenyl substituents, and the solid-state structure and computational modeling for the thienyl oxazine case.

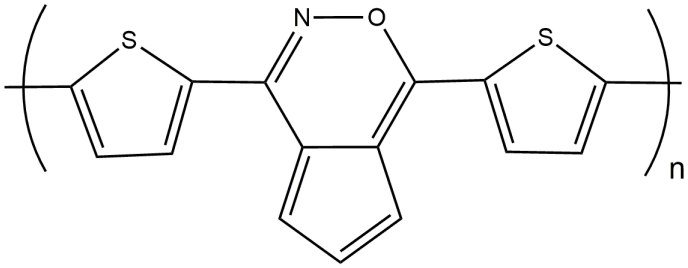

Figure 3. Envisioned thienylcyclopentaoxazine polymer

RESULTS AND DISCUSSION

Synthesis and Characterization

Two newly reported 1,4-disubstituted cyclopenta[*d*][1,2]oxazines (R = thienyl, 4-chlorophenyl) were formed using the route published by Linn and Sharkey.[25] (Figure 4) In a 3 to 2 ratio, lithium cyclopentadienide was reacted with the corresponding acid chloride to afford the 1,2-diacylcyclopentadiene (fulvene) precursor. These fulvenes were then ring closed by heating them in a solution of anhydrous pyridine/ethanol with hydroxylamine hydrochloride. This provided the desired substituted oxazines **1** and **2** in high yields (88.2 and 86.8% respectively). We attribute our increased yields compared to our previously reported series of oxazines[26] to more careful monitoring of the reaction mixture (via thin layer chromatography) to prevent thermal decomposition as well as adding additional hydroxylamine midway through the reaction time to improve conversion to the desired product. A total of 3 hour reaction times gave optimal yields for both oxazines **1** and **2**. While the 4-chlorophenyloxazine **2** displayed high stability in air and solution, thienyl **1** did show some evidence of instability under ambient conditions and would darken over a period of several days.

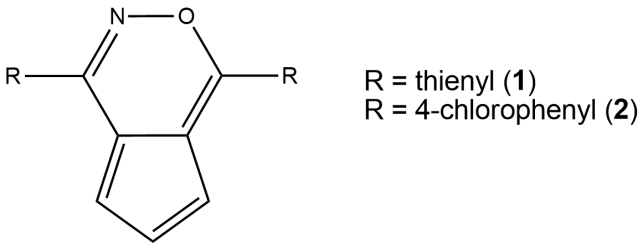

Figure 4. 1,4-Disubstituted cyclopenta[*d*][1,2]oxazines

^{1}H NMR spectroscopy confirms the structures for the oxazines **1** and **2** showing both asymmetric Cp and alkyl or aryl substituents. The range of chemical shifts (6.9-7.4 ppm) is typical for fused-ring Cp protons.[26,28,29] For oxazine **1**, the 3 separate Cp signals were not resolved and were observed as complex multiplet. However, for oxazine **2**, each unique Cp resonance was observed as a multiplet. Due to the lower solubility of **2** in chloroform-*d*, the spectrum was also obtained in DMSO-d_6. While the Cp

signals were resolved, we were still unable to observe coupling as theoretically predicted, observing only multiplets. As with our previous oxazine series, we attribute this complexity observed in coupling to the high degree of electron delocalization within the Cp ring. To demonstrate complete conversion on the fulvene starting material, we did not observe any trace of the characteristic "enolic" signals in the 18-20 ppm range. Also observed in the ^{13}C NMR spectroscopy were the cyclopentadiene ring carbons were, observed within a narrow range of 114-119 ppm. Characterization via IR spectroscopy of compounds **1** and **2** also showed the disappearance of the stretch at 3300 cm^{-1}, characteristic of an enolic stretch. The IR spectra for each oxazine displayed a set of newly formed N-O stretches at approximately a 1400 cm^{-1} and 1600 cm^{-1}. DART Mass Spectrometry also confirms the molecular structure of oxazines **1** and **2**, with the expected M^+ +1 ion peak observed for each case (a typical observance for positive scan mode in DART).[30] Elemental analysis was performed for both newly reported compounds as well. Both oxazines had observed Hydrogen and Nitrogen values that matched well with calculated values. For compound **2**, observed Carbon values also matched well with theoretical values. However, observed Carbon for compound **1** was slightly lower than calculated values, which we attribute to some air sensitivity of the thienyl case. This correlates well with the observed darkening of compound **1** in ambient atmosphere. Experimental details and characterization for both compounds **1** and **2** are given in the Experimental section.

X-Ray crystallographic analysis

The structure of the thienyl-oxazine **1** was further confirmed by single-crystal X-ray diffraction methods (Figure 5). Suitable crystals for analysis were grown by slow evaporation from a methylene chloride solution at ambient temperature and isolated as orange-red plates. Compound **1** crystallized with an orthorhombic lattice (space group $P2_12_12_1$), with two independent molecules in the asymmetric unit, and

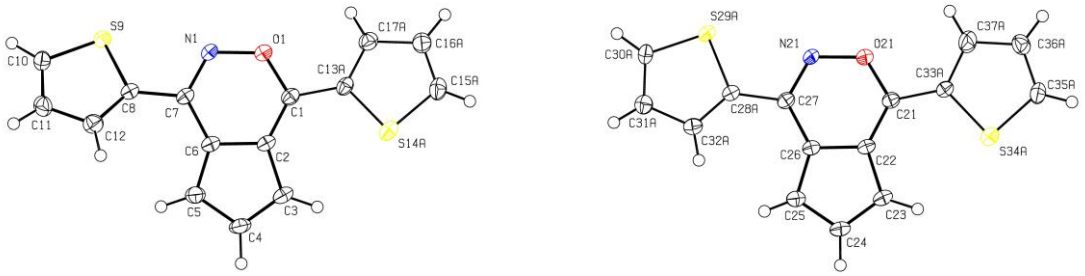

Figure 5. ORTEP stereographic projections of molecules **I** and **II** of the structure of thienyl-oxazine **1** at 120 K. Thermal ellipsoids are plotted at the 50% probability level. Only the major component of each of the disordered thienyl rings is plotted.

thus 8 molecules in the unit cell. The final refined model of the structure reveals that 3 of the 4 thienyl rings are disordered, with a minor component corresponding to a rotation of approximately 180° about the bond to the cyclopentaoxazine ring contributing approximately 10% to the total occupancy of each disordered ring site. The two molecules of the asymmetric unit show offset π-π stacking interactions with the cyclopentaoxazine ring of each molecule stacked above one of the thienyl rings of its neighbor. Short contacts are observed between both C32A and C2 and C32A and C6, with a distance less than the sum of the Van der Waals radii between the two unique molecules in the asymmetric unit (3.333(4) and 3.352(4) Å respectively). This differs from the π stacking observed in the previously reported structure of the tolyl substituted cyclopentaoxazine derivative,[26] where the cyclopentaoxazine rings of neighboring molecules are stacked above each other. In **I**, the molecular pair of molecules in the asymmetric unit are further packed in a herringbone pattern that propagates in the a lattice direction (Figure 6). Tables of crystallographic details, atomic coordinates and displacement parameters, bond distances and angles, intermolecular contact distances, structure factors and a crystallographic information file (CIF) for the structure of **I** have been deposited with the Cambridge Crystallographic Data Centre.[31]

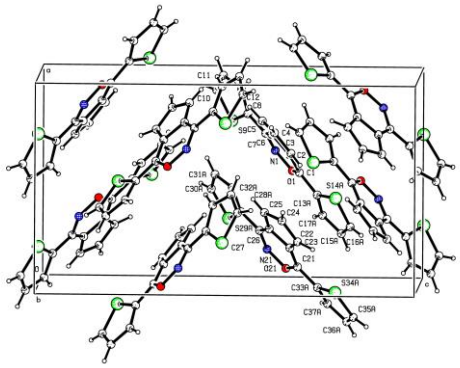

Figure 6. Projection of the packing in I viewed down the b axis

Computational studies

Geometric Optimization - All computations were performed using the Gaussian 16 program,[32] and Gauss-View 6 molecular visualization package[33] was used for processing the output. Geometry optimization was carried out with DFT methods in a series of steps starting with the B3 LYP density functional with a 631 basis set, and the final optimization presented here was calculated using the Perdew-Burke-Ernzerhof (PBE) generalized gradient exchange-correlation functional[34] and a triple-zeta correlation consistent (cc-pVTZ) basis[35] on the crystal structure data of oxazine **1**. The crystal structure has two unique molecules in the unit cell, so the optimization was performed starting with atomic coordinates of the molecule which possesses a more in-plane or flattened configuration (Molecule **II**). After optimization, a single point energy was found with the PBE functional with the cc-pVTZ basis to

ensure the lowest energy state. The optimized geometry were checked for imaginary frequencies with none being found. Table 1 gives selected torsional angles for the original molecules in the crystal structure and for the optimized geometry to compare the degree of planarity between the central oxazine ring and thienyl substituents. The optimized structure (Figure 7) displays the nitrogen-side thienyl being twisted out of plane and the oxygen-side being still close to an in-plane arrangement but twisted slightly below the plane of the oxazine ring (the 27-21-3-1 torsional angle transitioning from a positive value to a negative one). It is interesting to note the optimized geometry for the nitrogen-side thienyl more closely resembles the observed geometry of Molecule **I** in the crystal structure, with torsion angles 2-12-13-14 and 11-12-13-19 very similar (22.30° and 26.89° optimized vs. 22.8(3)° and 26.0° in Molecule **I**). Overall, the nitrogen-side thienyl orientation is more strongly twisted out of the plane compared to the original crystal structure and the oxygen-side thienyl is twisted in the opposite direction with respect to the central ring. This calculated geometry differs from the reported crystalline structure because the optimized structure is performed on a single molecule. The crystal structure is subject to multiple molecular interactions, which causes the rings to become more planer. For example, this analysis does not account for intermolecular interactions between those of Molecules **I** and **II** as seen in the crystal structure and only looks at the ideal geometry of the discrete molecule of interest. The nitrogen-side thienyl in Molecule **II** of the crystal structure is observed to have shorts contacts with the central oxazine ring of Molecule **I** (between C32A and C2 and C6). Thus, the greater planarity of this ring in the observed structure is likely due to optimizing this favorable intermolecular interaction.

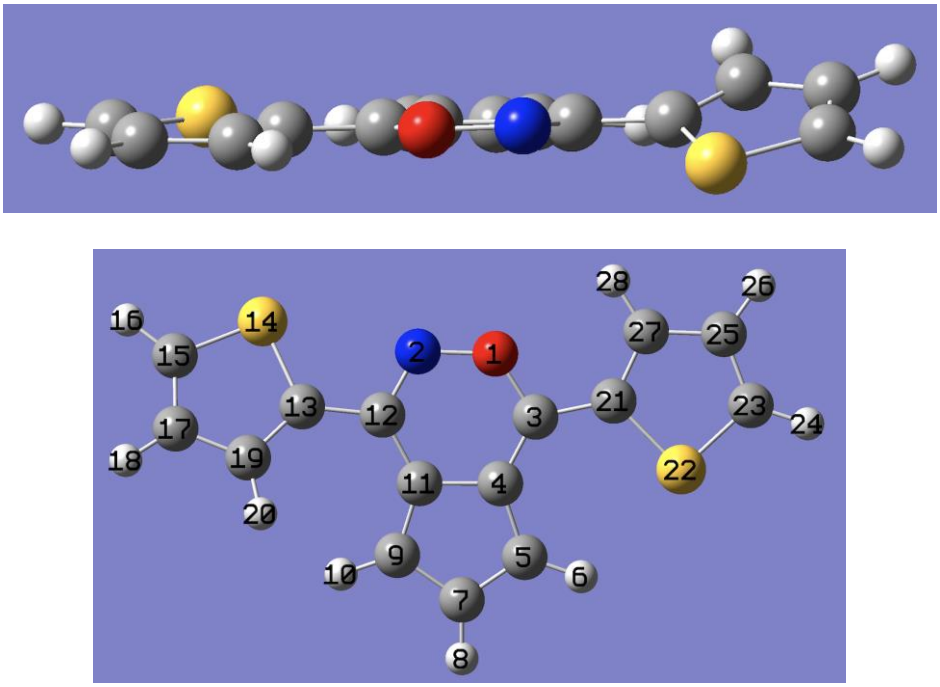

Figure 7. Optimized Geometry with labeled atoms

Table 1. Comparison of selected torsional angles (◦) from the X-ray crystal structure and the theoretical optimized structure. The atom labels are shown in Figure 5 for the crystal structure and Figure 7 for the theoretical calculation. Numbers in parentheses are estimated standard deviations in the last digit of the experimental value.

Oxygen side		
Crystal Molecule **I**	O1-C1-C13A-C17A	-12.9(4)
Crystal Molecule **II**	O21-C21-C33A-C37A	10.7(4)
Optimized Theory	27-21-3-1	-5.13
Crystal Molecule **I**	C2-C1-C13A-S14A	-16.0(3)
Crystal Molecule **II**	C22-C21-C33A-S34A	3.5(3)
Optimized Theory	22-21-3-4	-2.92
Crystal Molecule **I**	C13-C1-C2-C3	-6.8(4)
Crystal Molecule **II**	C33-C21-C22-C23	-1.8(3)
Optimized Theory	21-3-4-5	-2.92
Nitrogen side		
Crystal Molecule **I**	N1-C7-C8-S9	22.8(2)
Crystal Molecule **II**	N21-C27-C28-S29	8.1(2)
Optimized Theory	2-12-13-14	22.30
Crystal Molecule **I**	C6-C7-C8-C12	26.0(3)
Crystal Molecule **II**	C26-C27-C28-C32	10.8(3)
Optimized Theory	11-12-13-19	26.89
Crystal Molecule **I**	C5-C6-C7-C8	5.9(3)
Crystal Molecule **II**	C25-C26-C27-C28	4.5(3)
Optimized Theory	9-11-12-13	3.44

Electrostatic Potential Maps - To help visualize charge distributions and electronic properties, an electrostatic potential (ESP) map was created for the subject molecule using the PBE functional with the cc-pVTZ basis (Figure 8). This is a single surface counter (isovalue 0.004) and has the electrostatic potential plotted between -0.05 and +0.05. The red color (-0.05 eV) shows lower electrostatic potential values (electron-rich), and blue (+0.05 eV) higher values (electron-poor). The red regions indicate an area that would be ideal for nucleophilic (proton) binding and the blue regions are ideal for electrophilic (electron) binding. When looking at the ESP map for compound **1**, the red electron rich region is localized mainly on the nitrogen atom. The oxygen atom, the thienyl group on the nitrogen side, and the lower portion on the Cp ring (C5-C7-C9) are the next most electron rich regions indicated by the yellow color. When comparing relative electron density in the various portions of the oxazine, the thienyl ring containing the sulfur at position 22, (S14, the oxygen side) is the most electron poor. These regions would indicate that the solid state stacking of the molecule would best be optimized by having the oxygen-side thienyl over the electron rich central oxazine moiety. This orientation is what is observed

in the actual solid state structure, with the thienyl overlapping in such a fashion. The X-ray structure of compound **1** places the nitrogen-side thienyl of Molecule **I** in the unit cell stacked directly over the oxazine of Molecule **II** and the oxygen-side oxazine of Molecule **II** stacked over the oxazine portion of Molecule **I**. Overall, this mapping also helps to visualize the relative polarity of the molecule by the strong color difference between the nitrogen side and the thienyl on the oxygen side.

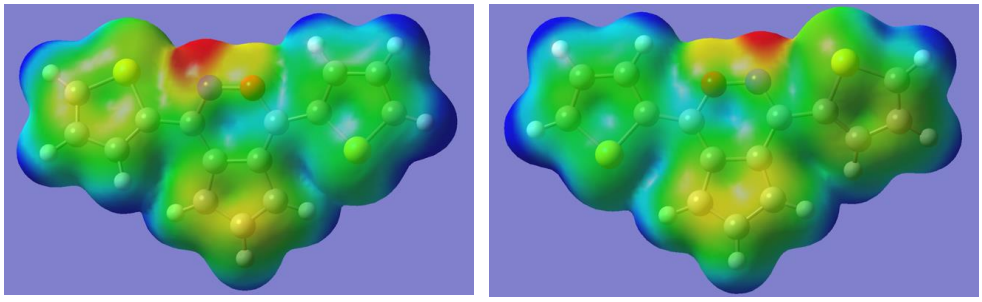

Figure 8. Front (left) and back (right) of molecule's ESP map

Natural Bond Analysis - A Natural Bond Orbital (NBO) analysis was done to help visualize and interpret electronic orbitals and further our understanding of intra- and intermolecular interactions of oxazine **1**. NBO analysis provides a more accurate form of orbitals, which are more Lewis type, to interpret for elementary bonding purposes.[28,36] These "natural Lewis orbitals" give the best depiction of where the highest electron density resides. Calculations were performed with PBE-cc-pVTZ methods using NBO 3.1.[37] The second order Fock matrix was calculated to examine the donor-acceptor interactions. A larger calculated stabilization energy indicates a stronger interaction between electron donors (Lewis Type) and acceptors (anti-bonding or Rydberg). These interactions show an overall delocalization of electron density which helps with stabilization.

There were several donor-acceptor pairs of interest in the NBO analysis. The first is the lone-pair of electrons on the oxygen (O1, Figure 9). These electrons interact with the neighboring antibonding carbon-carbon bond (C1-C2) and nitrogen-carbon bond (N1-C7). Furthermore, these interactions have stabilization energy values of 14.22 and 28.56 kcal/mol, which indicates a large delocalization of charge.

Figure 9. (O1) Lone-pair donor orbital and (N2-C12) as the anti-bonding acceptor orbital

Another observed stabilization for the system occurs when the lone pairs on the thienyl sulfur atom interacts with the thienyl carbon antibonding orbitals (Figure 10). For S9, there are interactions with C8-C12 and C10-C11 (17.35 and 18.44 kcal/mol) and S14 with C13-C17 and C15-C16 (16.94 and 18.21 kcal/mol).

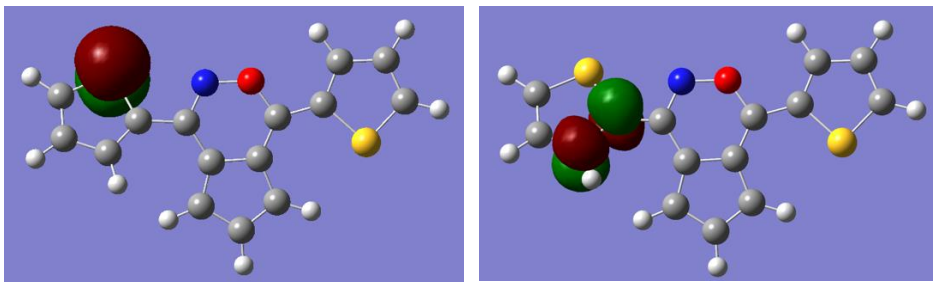

Figure 10. S14 Lone pair donating orbital and C13-C19 antibonding acceptor orbital

There is also a large number of interactions between the carbon orbitals on the thienyl rings. However, only strong stabilization energies between 11-29 kcal/mol are of interest. This is the recommended minimum threshold used on the NBO sorter program.[38] It is interesting to note that N1-C7 is an acceptor from C8-C12 and C5-C6, but the oxygen atom O1 does not participate in any acceptor orbitals. The overall orbital interactions in the oxazine are partitioned by the N1-C7 orbitals (Figures 11 and 12). The moiety containing S9 has donor-acceptor pairs that interact but stop at the N-C bond. Likewise, on the oxygen side, there is a large number of donor-acceptor pairs (6 donors and 7 acceptors) indicating a large delocalization of charge over the system. However, the N-C bond does not generally participate in the donor orbitals involving the oxygen oxazine. The sulfurs and oxygen heteroatoms only participate in donor interactions and are not involved with acceptor orbitals that stabilize the molecule, which is consistent with their electron rich nature. The charge separation seen in the ESP maps along with the extensive π-orbital interaction observed here are strong indicators that the material may be a good candidate for an NLO material. For example, both Zhang et al. and Tillekaratne et al. have shown that strong π-orbital interactions are a potential indicator of an NLO material.[39,40] These results are further confirmed with the HOMO-LUMO and hyperpolarizability calculations (see below).

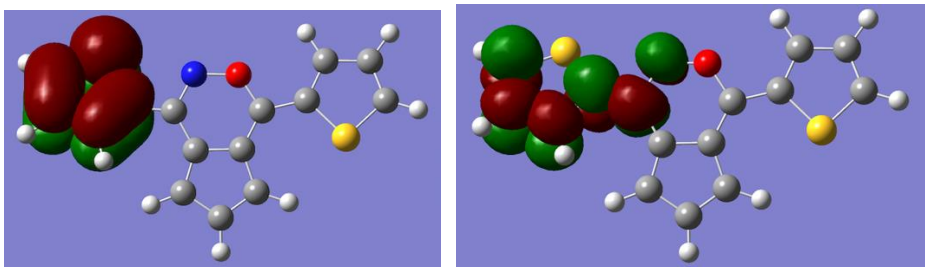

Figure 11. Donor (left) and acceptor (right) orbitals for the nitrogen side

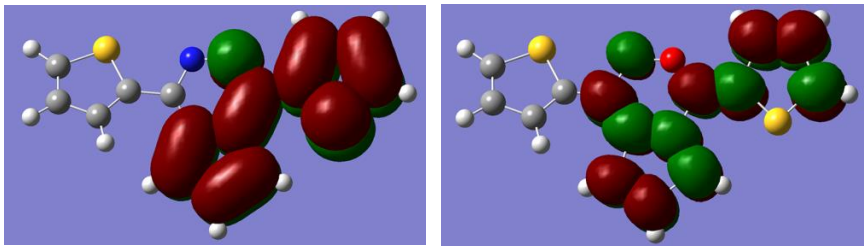

Figure 12. Donor (left) and acceptor (right) orbitals for the oxygen side

HOMO-LUMO Analysis - The HOMO-LUMO data shown was calculated using the Perdew-Burke-Ernzerhof (PBE) generalized gradient exchange-correlation functional[34] and a triple-zeta correlation consistent (cc-pVTZ) basis with canonical molecular orbitals. An image of the both the HOMO and LUMO is shown in Figure 13. While the HOMO encompasses the entirety of the molecule, the LUMO is composed mostly from orbital space on the central oxazine atom and oxygen-side thienyl. Again, it can be seen that the main orbitals involved are π-type, which is a good indicator of a potential NLO material.[39,40] The calculated HOMO-LUMO gap energy is 0.0942 a.u.. This relatively small gap is another strong sign of the material being favorable for NLO consideration.[41]

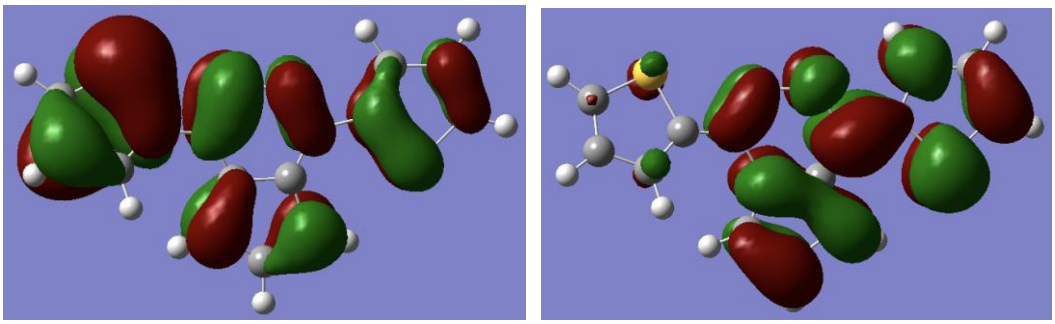

Figure 13. HOMO orbital (-0.31132 au) left and LUMO orbital (-0.21712 au) from the PBE cc-pVTZ

Hyperpolarizability - The first order hyperpolarizability is a tensor of rank 3 described by a 3x3x3 matrix. The 27 components of the 3D matrix can be reduced to 10 because of Kleinman symmetry.[42] The hyperpolarizability (β) values were calculated by the following equations using the Gaussian 16 output:

$$\beta = \left(\beta_x^2 + \beta_y^2 + \beta_z^2\right)^{1/2}$$

With

$$\beta_x = \beta_{xxx} + \beta_{xyy} + \beta_{xzz}$$
$$\beta_y = \beta_{yyy} + \beta_{xxy} + \beta_{yzz}$$
$$\beta_z = \beta_{zzz} + \beta_{xxz} + \beta_{yyz}$$

The calculated β value for the compound are shown in Table 2. The total β value was 9.9 x10^{-30} esu (electrostatic units). A common standard for comparison with hyperpolarizability values is urea, which has a value of 2.3x10-30 esu.[43] Thus, the reported compound has a value 4 times larger than urea, which indicates that this thienyl oxazine would be suitable for NLO applications. Furthermore, these results agree with other reported work on various thiophene-based materials that show these heterocycles have strong potential as NLO materials.[44,45] Thiophene substituted molecules have even been shown to have better NLO properties then the original non-heterocyclic structures.[46] We also note that the largest value for Beta was β_{xxy}, which indicates the direction of charge transfer in the molecule (Figure 14).

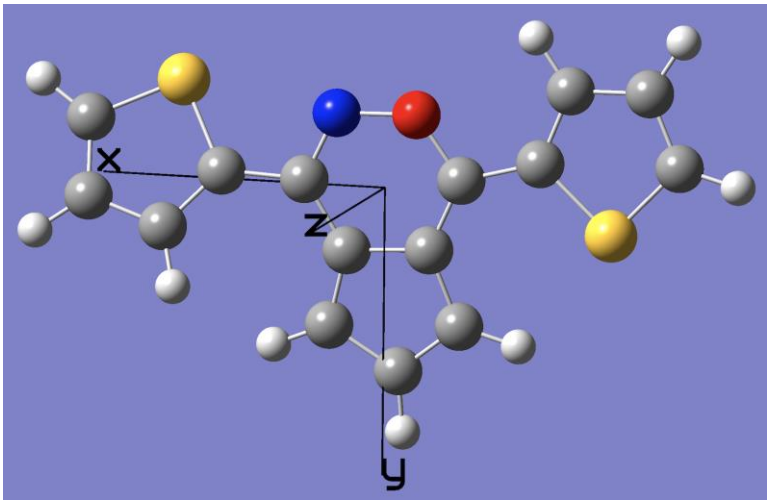

Figure 14. Structure of compound **1** with coordinate axis

Table 2. Calculated hyperpolarizability for the thienyl-oxazine molecule

	$\beta_{components}$ $(x10^{-30}esu)$
xxx	-9.9593
xxy	4.651546
xyy	0.419883
yyy	-1.60076
xxz	-0.3627
xyz	0.288864
yyz	0.022668
xzz	0.169263
yzz	0.156219
zzz	0.019705
Total	9.9089

Overall, the strong potential for NLO applications are supported by our reported calculations. Along with the hyperpolarizability, the ESP maps show a charge distribution which favors a dipole in the system. The NBOs for compound **1** indicate strong charge mobility in the π electrons, which is also a critical

indicator for potential NLO materials.[44-46] Additionally, the small HOMO-LUMO energy gap further suggests favorable NLO applications.[41]

EXPERIMENTAL

All reactions were carried out using standard Schlenk techniques under a nitrogen atmosphere unless otherwise noted. NMR solvent chloroform-*d* (Acros) and DMSO-d_6 (Cambridge Isotope Laboratories), hydroxylamine hydrochloride, magnesium sulfate (Alfa Aesar), anhydrous pyridine, anhydrous EtOH, hexanes, pentane, and CH_2Cl (Aldrich) were all used without further purification. The 1,2-diacylcyclopentadiene precursors were all made according to previously reported procedures.[25,47] ^1H and ^{13}C NMR spectra were recorded on a Bruker 400 MHz NMR spectrometer at ca. 22 °C and were referenced to residual solvent peaks and TMS internal standard. All ^{13}C NMR spectra were listed as decoupled. All infrared spectra were recorded on a Perkin Elmer Spectrum One FT-IR Spectrometer. The mass spectrometry analysis was performed with a Direct Analysis in Real Time SVP ion source (IonSense, Saugus, MA, USA) interfaced with a LTQ XL linear ion trap mass spectrometer (Thermo Scientific, San Jose, CA, USA). Specific details for this system and operation have been previously reported.[30] All data reported here are under Positive Scan mode. Melting points were taken on a standard Mel-Temp apparatus.

Synthesis of 1,4-di(thiophen-2-yl)cyclopenta[d][1,2]oxazine (1) In a 25-mL round bottom flask, a solution of 1,2-dithienylcyclopentadiene (251.4 mg, 0.879 mmol) and hydroxylamine hydrochloride (250.6 mg, 3.626 mmol, 6 mol. eq.) in 5 mL absolute EtOH and 5 mL anhydrous pyridine was refluxed for 3 h. An additional 248.5 mg of hydroxylamine was added at 1.5 h to drive the reaction to completion. The orange brown reaction mixture was then quenched with water and extracted with CH_2Cl_2. The organic fractions were collected, dried over $MgSO_4$, filtered, and the volatiles were then removed *in vacuo*. The crude product was then triturated with hexanes to afford **1** as brick orange solid (202.0 mg, 88.2%). **Mp** 78-84 °C. **^1H NMR (400 MHz, $CDCl_3$, ppm):** 7.33 (m, 3H, Cp), 7.35 (t, 1H, J_3 = 3.2 Hz, Tp), 7.40 (d, 1H, J_3 = 4.8 Hz, Tp), 7.54 (d, 1H, J_3 = 4.8 Hz, Tp), 7.71 (d, 1H, J_3 = 4.4 Hz, Tp), 7.88 (d, 1H, J_3 = 4.0 Hz, Tp), 8.06 (d, 1H, J_3 = 3.2 Hz, Tp). **^{13}C NMR (100 MHz, $CDCl_3$, ppm):** 114.9, 115.4, 116.9, 117.2, 127.8, 128.5, 128.9, 131.4, 132.1, 133.4, 134.8, 135.1, 150.5, 159.4. **IR (cm^{-1}):** 1382, 1598 (strong, N-O). **MS(DART-LTQ):** *m/z* 284.08 (M^+ + 1). Anal. Calcd for $C_{15}H_9NOS_2$: C, 63.6; H, 3.2; N, 4.9. Found: C, 62.1; H, 3.4; N, 5.2.

The crystal structure of **1** was determined from single-crystal X-ray diffraction intensity measurements. An orange-red crystal, typical of others in a batch grown by slow evaporation from a CH_2Cl_2 solution at room temperature, was selected for data collection. The crystal was mounted on a MiTeGin microloop with dodecane oil and cooled to 120 K in a stream of cold N_2 gas generated using an Oxford Cryosystems

700 low temperature device. Data were collected at 120 K with a Bruker APEX II Kappa CCD diffractometer. The APEX II software package was used for indexing, data collection and reduction, and for determination of an empirical absorption correction.[48] The SHELXS/L software package was used for structure solution and refinement.[49] Hydrogen atoms were located in difference Fourier maps and included in the least-squares refinement with isotropic thermal parameters. Unreasonable anisotropic thermal parameters, residual peaks in difference Fourier maps, and an unexpectedly high *R*-factor suggested the possibility of disorder in the orientation of 3 of the 4 thienyl rings. To improve the fit to the X-ray data, a disordered model was employed in which a second orientation for each of the disordered thienyl rings (indicated by the letter B on the atom labels) was included rotated by approximately 180° about the bond to the cyclopentaoxazine ring with an initial occupancy of 0.100. The sum of the major and minor occupancies of each disordered ring were constrained to equal 1.000 for each disordered molecular site, and the occupancies were refined in the full SHELX refinement. Distance similarity restraints were imposed on the bonds and angles of the disordered thienyl ring atoms to ensure a high degree of structural similarity between the two molecular orientations of each disordered ring. Similarity restraints were also imposed on the thermal parameters of atoms in the disordered rings, hydrogen atoms for the minor disordered ring component were included at calculated positions, and the relative occupancy of each disordered ring was refined independently. Refinement of the disordered model with 9518 X-ray structure factors improved the fit to the X-ray data from R_1= 0.0452 to R_1=0.0342 for observations with I > 2σ(I), yielding occupancy factors of 0.890(3), 0.920(3) and 0.876(3) for the major components of the thienyl rings containing S(14), S(29) and S(34), respectively. Crystal data and a summary of experimental
details are given in Table 3.

Table 3. Sample and crystal data for compound **1**

Chemical formula	$C_{15}H_9NOS_2$	
Formula weight	283.35 g/mol	
Temperature	120(2) K	
Wavelength	0.71073 Å	
Crystal size	0.10 x 0.20 x 0.20 mm	
Crystal habit	Clear orange-red plate	
Crystal system	Orthorhombic	
Space group	$P2_12_12_1$	
Unit cell dimensions	a = 10.5957(9) Å	α = 90°
	b = 12.2292(11) Å	β = 90°
	c = 19.2479(17) Å	γ = 90°

Volume	2494.1(4) $Å^3$
Z	8
Density (calculated)	1.509 g/cm^3
Absorption coefficient	0.415 mm^{-1}
F(000)	1168
Theta range for data collection	1.97 to 33.18°
Index ranges	$-16 \le h \le 16$, $-18 \le k \le 13$, $-29 \le l \le 29$
Reflections collected	77504
Independent reflections	9518 [R(int) = 0.0355]
Coverage of independent reflections	99.9%
Absorption correction	Multi-Scan
Max. and min. transmission	0.8624 and 0.8172
Refinement method	Full-matrix least-squares on F^2
Function minimized	$\Sigma\, w(F_o^2 - F_c^2)^2$
Data / restraints / parameters	9518 / 732 / 521
Goodness-of-fit on F^2	1.037
Δ/σ_{max}	0.008
Final *R* indices	8802 data; $I>2\sigma(I)$ $R_1 = 0.0342$, $wR_2 = 0.0883$ All data; $R_1 = 0.0388$, $wR_2 = 0.0914$
Weighting scheme	$w=1/[\sigma^2(F_o^2)+(0.0503P)^2+0.6344P]$ where $P=(F_o^2+2F_c^2)/3$
Absolute structure parameter	-0.07(3)
Largest diff. peak and hole	0.522 and -0.437 $eÅ^{-3}$
RMS deviation from mean	0.052 $eÅ^{-3}$

Synthesis of 1,4-di-p-chlorophenylcyclopenta[d][1,2]oxazine (2) In a 25-mL round bottom flask, a solution of 1,2-di-*p*-chlorophenylcyclopentadiene (253.7 mg, 0.740 mmol) and hydroxylamine hydrochloride (253.7 mg, 3.671 mmol, 6 mol. eq.) in 5 mL absolute EtOH and 5 mL anhydrous pyridine was refluxed for 3 h. An additional 250.0 mg of hydroxylamine was added at 1.5 h to drive the reaction to completion. The yellow brown reaction mixture was then quenched with water and extracted with CH_2Cl. The organic fractions were collected, dried over $MgSO_4$, filtered, and the volatiles were then removed *in vacuo*. The crude product was then triturated with pentane to afford 2 as yellow solid (213.9 mg, 86.8%). **Mp** 189-191 °C. **^{1}H NMR (400 MHz, DMSO-d_6, ppm):** 7.01 (m, 1H, Cp), 7.34 (m, 1H, Cp), 7.42 (m, 1H, Cp), 7.65 (d, 2H, J_3 = 8.0 Hz, Ar), 7.73 (d, 2H, J_3 = 8.4 Hz, Ar), 7.88 (d, 2H, J_3 = 8.4 Hz, Ar), 8.12 (d, 2H, J_3 = 8.0 Hz, Ar). **^{1}H NMR (400 MHz, $CDCl_3$ ppm):** 6.94 (m, 1H, Cp), 7.24 (m, 1H, Cp), 7.38 (m, 1H, Cp), 7.53 (d, 2H, J_3 = 8.4 Hz, Ar), 7.58 (d, 2H, J_3 = 8.4 Hz, Ar), 7.84 (d, 2H, J_3 = 8.4

Hz, Ar), 8.04 (d, 2H, J_3 = 8.4 Hz, Ar). **^{13}C NMR (100 MHz, CDCl$_3$, ppm):** 115.7, 117.4, 118.4, 129.2, 129.5, 130.1, 130.2, 130.4, 132.0, 135.4, 136.5, 138.4, 155.4, 164.4. **IR (cm^{-1}):** 1382, 1615 (strong, N-O). **MS(DART-LTQ):** *m/z* 340.42 (M^+ + 1). Anal. Calcd for $C_{19}H_{11}NOCl_2$: C, 67.1; H, 3.3; N, 4.1. Found: C, 67.3; H, 3.3; N, 4.2.

ACKNOWLEDGEMENTS

We wish to thank our sources of support for this research, including the Department of Physical Sciences and the Faculty Development Committee at the University of Findlay.

REFERENCES AND NOTES

1. A. R. Katritzky and C. W. Rees, 'Comprehensive Heterocyclic Chemistry: Structure, Reactions, Synthesis and Uses of Heterocyclic Compounds', Pergamon, Oxford, 1984.
2. P. Dallemagne, L. P. Khanh, A. Alsaidi, O. Renault, I. Varlet, V. Collot, R. Bureau, and S. Rault, *Bioorg. Med. Chem.*, 2002, **10**, 2185.
3. P. Dallemagne, L. P. Khanh, A. Alsaidi, I. Varlet, V. Collot, M. Paillet, R. Bureau, and S. Rault, *Bioorg. Med. Chem.*, 2003, **11**, 1161.
4. L. P. Khanh, P. Dallemagne, H. Landelle, and S. Rault, *J. Enzym. Inhib. Med. Chem.*, 2002, **17**, 439.
5. L. P. Khanh, P. Dallemagne, and S. Rault, *Synthesis*, 2002, 1091.
6. M. Oh, J. A. Reingold, G. B. Carpenter, and D. A. Sweigart, *Coord. Chem. Rev.*, 2004, **248**, 561.
7. L. M. Tolbert, *Acc. Chem. Res.*, 1992, **25**, 561.
8. J. Bredas, A. J. Heeger, and F. Wudl, *Chem. Phys.*, 1986, **85**, 4673.
9. J. Roncali, *Chem. Rev.*, 1997, **97**, 173.
10. J.-F. Tremblay, *Chem. Eng. News*, 2016, **94**, 25.
11. M. Jacoby, *Chem. Eng. News*, 2016, **94**, 30.
12. I. Sheikhshoaie, F. Belaj, and A. Kamali, *Bull. Chem. Soc. Ethiop.*, 2010, **24**, 283.
13. A. Y. Sukhoruko, A. C. Nirvanappa, J. Swamy, S. L. Ioffe, S. N. Swamy, Basappa, and K. S. Rangappa, *Bioorg. Med. Chem. Lett.*, 2014, **24**, 3618.
14. V. Srinivas, C. D. Mohan, C. P. Baburajeev, S. Rangappa, S. Jagadish, J. E. Fuchs, A. Y. Sukhorukov, Chandra, D. J. Mason, K. S. S. Kumar, M. Madegowda, A. Bender, Basappa, and K. S. Rangappa, *Bioorg. Med. Chem. Lett.*, 2015, **25**, 2931.
15. S. Y. Cho, J. Y. Baek, S. S. Han, S. K. Kang, J. D. Ha, J. H. Ahn, J. D. Lee, K. R. Kim, H. G. Cheon, S. D. Rhee, S. D. Yang, G. H. Yon, C. S. Pak, and J.-K. Choi, *Bioorg. Med. Chem. Lett.*, 2006, **16**, 499.
16. M. Hannus, C. Martin, M. M. Mota, M. Prudencio, and C. D. Rodrigues, 'Use of inhibitors of

scavenger receptor class proteins for the treatment of infectious diseases'. WO 2007101710 A1 20070913, 2007.

17. S. D'Andrea, Z. B. Zheng, K. DenBleyker, J. C. Fung-Tomc, H. Yang, J. Clark, D. Taylor, and J. Bronson, *Bioorg. Med. Chem. Lett.*, 2005, **15**, 2834.
18. Y. Lin, Z. Shao, G. Jiang, S. Zhou, J. Cai, L. L. P. Vrijmoed, and E. B. G. Jones, *Tetrahedron*, 2000, **56**, 9607.
19. D. Lloyd and N. W. Preston, *J. Chem. Soc. (C)*, 1970, 610.
20. R. Lebeuf, I. Ferezou, J. Rossier, S. Arseniyadis, and J. Cossy, *Org. Lett.*, 2009, **11**, 4822.
21. A. J. Jenkins, Z. Mao, A. Kurimoto, L. T. Mix, N. Frank, and D. S. Larson, *J. Phys. Chem. Lett.*, 2018, **9**, 5351.
22. A. Kongkanand and P. V. Kamat, *ACS Nano*, 2007, **1**, 13.
23. M. Rickwood, S. Marsden, M. Ormsby, A. Staunton, D. Wood, J. Hepworth, and C. D. Gabbutt, *Mol. Cryst. Liq. Cryst.*, 1994, **1**, 17.
24. E. Gilbert, M. Taverna, M. Dieser, G. Morales, M. Sponton, and D. Estenoz, *J. Polym. Res.*, 2018, **114**, 1.
25. W. J. Linn and W. H. Sharkey, *J. Am. Chem. Soc.*, 1957, **79**, 4970.
26. N. Tice, E. Collins, D. Smith, C. Snyder, B. Yan, and E. Stevens, *J. Heterocycl. Chem.*, 2017, **54**, 3235.
27. R. Elsenbaumer and J. Reynolds, 'Handbook of Conducting Polymers', Marcel Dekker Inc., New York, 1998.
28. C. Snyder, N. Tice, J. Maddox, S. Parkin, A. Daniel, and J. Thomas, *Heterocycles*, 2011, **83**, 1275.
29. C. Snyder, N. Tice, P. Sriramula, J. Neathery, J. Mobley, C. Phillips, A. Preston, J. Strain, E. Vanover, M. Starling, N. Sahi, and K. Bunnell, *Synth. Commun.*, 2011, **41**, 1357.
30. M. Mazzotta, J. Young, J. Evans, L. Dopierala, Z. Claytor, A. Smith, C. Snyder, N. Tice, and D. Smith, *Anal. Methods*, 2015, **7**, 4003.
31. CCDC 1921512 contains the supplementary crystallographic data for this paper. These data can be obtained free of charge from The Cambridge Crystallographic Data Centre via www.ccdc.cam.ac.uk/data_request/cif.
32. Gaussian 16, Revision B.01, M. Frisch, G. Trucks, H. Schlegel, G. Scuseria, M. Robb, J. Cheeseman, G. Scalmani, V. Barone, G. Petersson, H. Nakatsuji, X. Li, M. Caricato, A. V. Marenich, J. Bloino, B. Janesko, R. Gomperts, B. Mennucci, H. Hratchian, J. Ortiz, A. Izmaylov, J. Sonnenberg, D. Williams-Young, F. Ding, F. Lipparini, F. Egidi, J. Goings, B. Peng, A. Petrone, T. Henderson, D. Ranasinghe, V. Zakrzewski, J. Gao, N. Rega, G. Zheng, W. Liang, M. Hada, M. Ehara, K. Toyota, R. Fukuda, J. Hasegawa, M. Ishida, T. Nakajima, Y. Honda, O. Kitao, H. Nakai, T. Vreven, K.

Throssell, J. A. Montgomery, Jr., J. Peralta, F. Ogliaro, M. Bearpark, J. Heyd, K. Brothers, V. Kudin, T. Staroverov, R. Keith, J. Kobayashi, K. Normand, E. Raghavachari, A. Rendell, J. Burant, S. Iyengar, J. Tomasi, M. Cossi, J. Millam, M. Klene, C. Adamo, R. Cammi, J. Ochterski, R. Martin, K. Morokuma, O. Farkas, J. B. Foresman, and D. Fox, Gaussian, Inc., Wallingford CT, 2016.

33. GaussView, Version 6, R. Dennington, T. Keith, and J. Millam, Semichem Inc., Shawnee Mission, KS, 2016.
34. J. Perdew, K. Burke, and M. Ernzerhof, *Phys. Rev. Lett.*, 1996, **77**, 3865.
35. T. Dunning Jr., *J. Chem. Phys.*, 1989, **90**, 1007.
36. A. Reed, L. Curtiss, and F. Weinhold, *Chem. Rev.*, 1988, **88**, 899.
37. NBO Version 3.1: E. Glendening, A. Reed, J. Carpenter, and F. Weinhold.
38. https://computational-chemistry.com/en/blog/visualization-of-nbo-on-gauss-view/
39. A. D. Tillekaratne, R. M. de Silva, and K. M. N. de Silva, *J. Mol. Struct.*, 2003, **638**, 169.
40. R. Zhang, B. Du, G. Sun, and Y. Sun, S*pectrochim. Acta A: Mol. Biomol. Spectrosc.*, 2010, **75**, 1115.
41. K. Öberg, A. Berglund, U. Edlund, and B. Eliasson, *J. Chem. Inf. Comput. Sci.*, 2001 **41**, 811.
42. D. Kleinman, *Phys. Rev.*, 1962, **126**, 1977.
43. C. Cassidy, J. Halbout, W. Donaldson, and C. Tang, *Opt. Commun.*, 1979, **29**, 243.
44. T. Abbaz, A. Bendjeddou, and D. Villemin, *Arc. Curr. Res. Int.*, 2018, **14**, 1.
45. A. Mahmood, S. Khan, U. Rana, M. Janjua, M. Tahir, M. Nazar, and Y. Song, *J. Phys. Org. Chem.*, 2015, **28**, 418.
46. E. Breitung, C. Shu, and R. McMahon, *J. Am. Chem. Soc.*, 2000, **122**, 1154.0
47. N. Tice, 'The synthesis, structure, and reactivity of some organometallic–fused heterocycles'. Ph.D. Thesis, Department of Chemistry, University of Kentucky, Lexington, 2006.
48. *Bruker APEX II*, 2012, Bruker AXS Inc., Madison, Wisconsin, USA.
49. G. M. Sheldrick, *Acta Crystallogr., Sect. C*, 2015, **71**, 3.